X-RAY SPECTROMETRY VOL.

Microbeam-Forming Methods for Synchrotron Radiation

G.E. Ice
Metals and Ceramics Division, Oak Ridge National Laboratory, Oak Ridge TN 37831-6118

The increasing availability of synchrotron x-ray sources has stimulated the development of advanced hard x-ray (E≥ 5 keV) microprobes. It is now possible to achieve intense submicron x-ray beams with a variety of techniques including Fresnel zone plates, Kirkpatrick-Baez mirrors, tapered capillaries and Bragg-Fresnel optics. These synchrotron based x-ray microprobes can be used for ultra-sensitive elemental detection by x-ray fluorescence/absorption and for microdiffraction to identify phase and strain with submicron resolution. Advanced methods for micro-beam forming are reviewed and the relative merits of each approach are discussed. The efficient techniques developed for synchrotron beams can also be used to tailor the beam properties from conventional x-ray sources.

Introduction

.

Techniques for developing x-ray microbeams from synchrotron radiation sources have been previously reviewed,[1-6] but the field is being revolutionized by recent developments.[7-16] New methods have been recently devised for controlling the surface figure of ultra-smooth x-ray mirrors.[7-9] New techniques have also been developed for the deposition of synthetic layered and zone plate structures.[10-13] Also there has been progress in the art and science of drawing tapered glass capillaries.[14-16] These major advances in x-ray optics have been driven by the increasing availability of powerful synchrotron radiation sources and by the promise of an intense x-ray microprobe.

Synchrotron sources can be 8-12 orders of magnitude more brilliant than the best conventional sources, and the achievable x-ray microbeam intensity is ultimately set by source brilliance : brilliance is defined as the photon flux per unit source area, per unit solid angle , per unit energy (e.g. $ps^{-1}eV^{-1}mm^{-1}mrad^{-1}$). This enormous advance in source brilliance is sufficient to allow the development of submicron x-ray probes with unique capabilities.

For example, x-ray excitation has been shown[17] to have higher fluorescent yields and much larger signal-to-noise than charged particle excitations. This results in approximately 10^{-4} less energy deposited in the sample for the same elemental detectability and orders of magnitude lower minimum detectable limits when incident photon intensities ≥ 10^8 photons $\mu m^{-2}s^{-1}$ are achieved.

X-ray microbeams are also highly desired for x-ray microdiffraction experiments: x-ray diffraction can allow strain resolution of better than 1 part to 10^4 and can operate as a nondestructive penetrating probe.[18,19] The inherent advantages of x-rays and the recent advances in sources and x-ray optics have

set the stage for a new generation of advanced x-ray microprobes.

Sources

Although the advantages of an x-ray microprobe have been recognized for at least 30 years, weak sources and inefficient x-ray optics have limited their widespread application. The development of intense synchrotron x-ray sources in the 70's provided beams less intense than electron sources, but 3 to 6 orders of magnitude more intense than conventional x-ray sources.

Early (first generation) sources were parasitic to high energy physics programs. These sources utilized the swath of radiation emitted during the radial acceleration of relativistic charged particles in synchrotron or storage rings. First generation synchrotron sources had relatively large source size, with unstable beam properties (Fig. 1a). Dedicated second generation sources were constructed with greatly enhanced x-ray brilliance achieved by shrinking the source dimensions (Fig. 1b) and increasing the charged particle current. Third generation sources further enhanced source brilliance by incorporating special magnetic structures called undulators, which produce highly collimated x-ray beams with tunable spectral peaks (Fig. 1c).

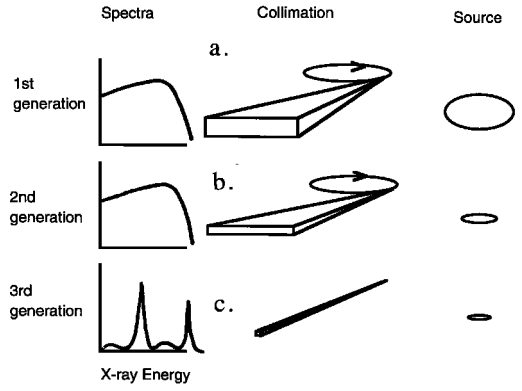

Fig. 1 The three generations of x-ray synchrotron sources.

Early Synchrotron X-ray Microprobes

In 1972 the first x-ray microscope/microprobe on a synchrotron source was reported by Horowitz and Howells.[20] Using a 2 μm pinhole and an ellipsoidal quartz condensing mirror, they instrumented a fluorescent/transmission soft x-ray microscope on the now dismantled Cambridge Electron Accelerator. This first effort at a synchrotron-based x-ray microprobe demonstrated many of the inherent advantages of x-rays for an advanced microprobe: operation in air, deep penetration into the sample, and sensitivity to atomic number.

In the mid 70's Sparks and co-workers began quantifying the minimum detectable limits achievable using synchrotron radiation to excite fluorescence.[21] They found that the signal-to-noise was orders of magnitude better for synchrotron excited fluorescence than for charged particle excited fluorescence (Fig. 2).

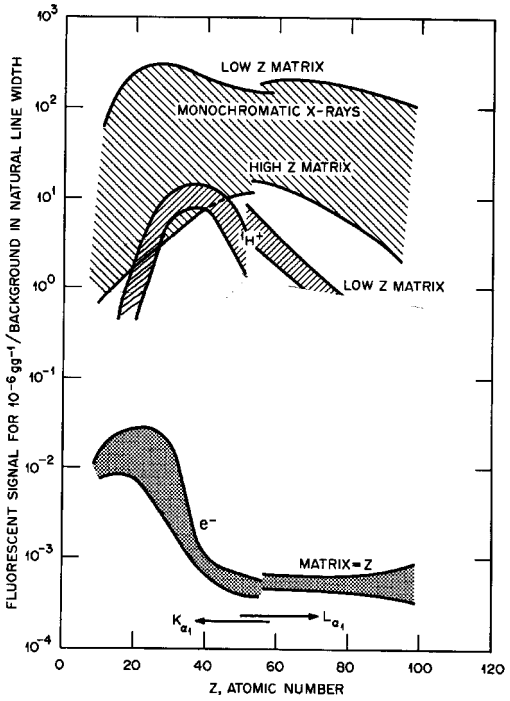

Fig. 2 Signal-to-noise from synchrotron x-rays compared to charged particles (after reference 17).

In 1977, based on this work, a pioneering x-ray microprobe was instrumented on

the Stanford Synchrotron Radiation Project.[22,23] This microprobe was designed to test the reported discovery of primordial superheavy elements (113 <Z<128).[24] A curved mosaic graphite monochromator focused the beam to a flux density of 10^{10} 37 keV photons/sec/mm^2. With this probe, small (30-150 μm) crystalline monazite inclusions were studied with two orders of magnitude greater elemental sensitivity to Z=126 than could be obtained using proton induced fluorescence and with much less sample heating. The measurements demonstrated that at a concentration level of 5 x 10^8 atoms per inclusion (5-500 ppb), the reported superheavy elements were not observable (Fig. 3).

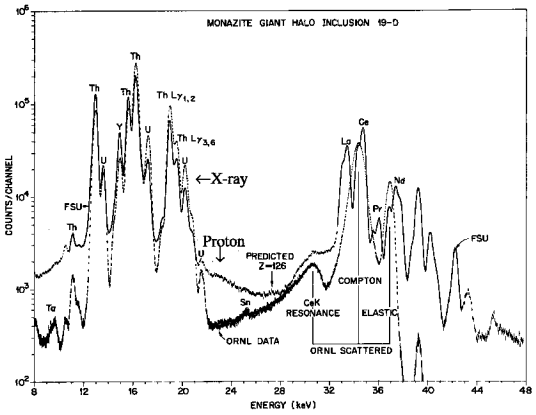

Fig. 3 Comparison of x-ray (ORNL) and proton excited spectra from monozite inclusions reported to contain super heavy elements. There is no evidence of a super heavy element fluorescent line in the x-ray excited spectra at 5 x10^8 atoms.

This convincing experimental demonstration that superheavy elements did *not* exist in concentrations far below those reported from proton microbeam experiments spared countless theorists and experimenters from embarking on a crash program to isolate and understand the origin and nature of superheavy atoms.

Since these pioneering experiments, synchrotron sources have continued to gain in x-ray brilliance and x-ray focusing optics have continued to evolve. As shown in Fig. 4 the x-ray brilliance has been doubling every 9 months since the 70's. With the completion of new third generation synchrotron sources, the x-ray brilliance will improve an additional 3 to 5 orders of magnitude over second generation sources. We are now poised at the beginning of a new era for x-ray microbeams where the achievable flux density on the sample is limited by sample heating and by the efficiency of the optics.

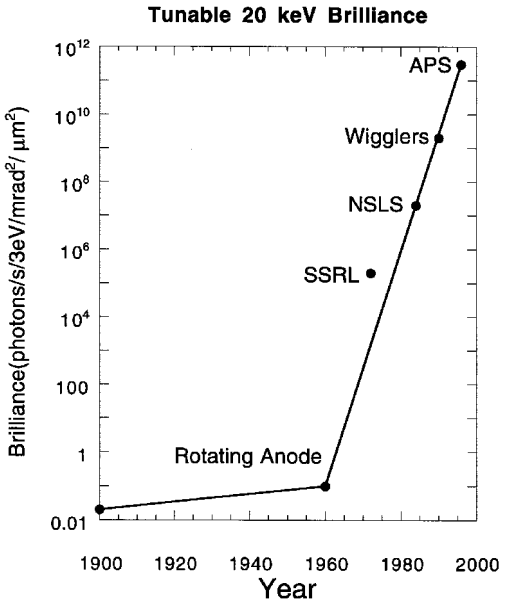

Fig. 4 X-ray source brilliance has risen exponentially as a function of time.

X-ray microbeam optics have been rapidly improving to efficiently use intense synchrotron beams. Ingenuity in x-ray optics has been driven both by new experimental opportunities and by the need for increased optical perfection; more perfect focusing is required to preserve brilliance and small image size at increasingly long object distances. We review briefly the basic principles of x-ray optics to appreciate the dramatic recent developments in x-ray microforming methods.

Fundamentals of X-ray Focusing Optics

The Wave Nature of X-rays

All x-ray optics make use of the wave nature of x-rays. Whereas visible light has a wavelength of around 600 nm, the wavelength of x-rays is around 0.1 nm and is related to the x-ray energy by,

$$E(keV) = 1.2398/\lambda(nm). \qquad (1)$$

Here the x-ray energy E is in kiloelectron volts and the wavelength ,λ, is in nanometers. Although x rays obey the same optical laws as visible light, their vastly different interaction with matter and their four orders of magnitude shorter wavelength presents different opportunities and challenges for focusing.

For x rays the index of refraction is less in matter than in a vacuum and is so close to unity that refractive optics are impractical.[25] Away from resonant absorption edges, the index or refraction for 10 keV x-rays is given by

$$n \sim 1 - \delta . \qquad (2)$$

Here δ is on the order of 10^{-5}-10^{-6}. Although this small δ precludes refractive optics, the path of an x-ray photon can be controlled by interference devices like crystals , multilayers and zone plates, or by reflection from smooth surfaces.

Total external reflection is one of the most useful tools for microfocusing optics. With total *external* reflection mirrors, x-rays are specularly reflected from ultra smooth surfaces. This process is equivalent to total *internal* reflection at visible wavelengths where the index of refraction is smaller in vacuum than in the transparent media . For a heavy Z mirror the critical angle below which total *external* reflection occurs is θ_C(rad)~0.08/E(keV). As illustrated below in Fig. 5a, reflectivity can be nearly unity for incident x-ray beams below the critical angle. Mirror reflection is especially useful for focusing broad bandpass radiation.

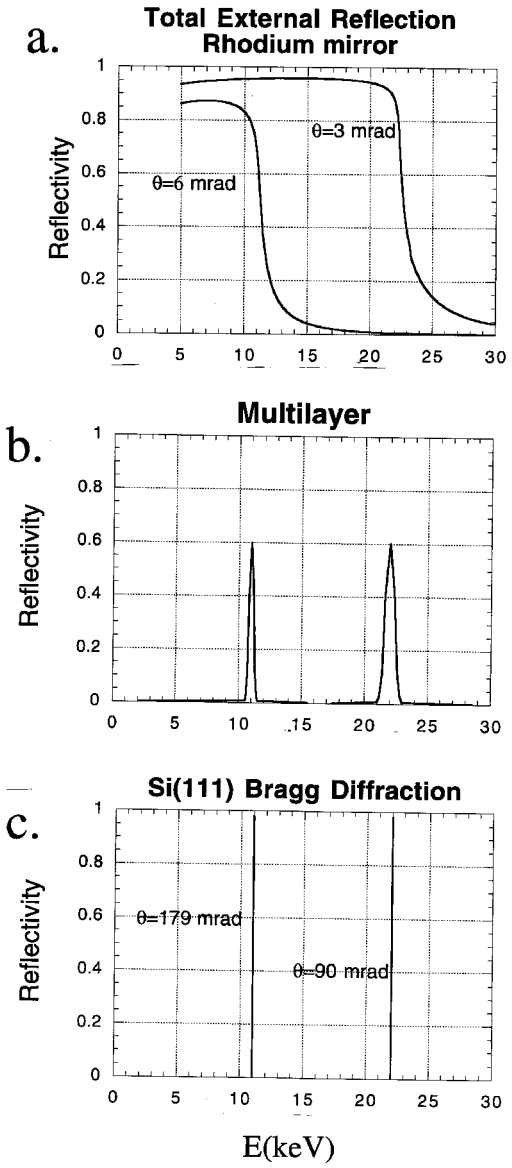

Fig. 5 X-ray reflection from (a) total external reflection mirrors, (b) multilayers, (c) diffracting single crystals.

X-rays can also be reflected by diffraction from the atomic planes of crystals. Although the scattering from each atomic plane is weak, at the Bragg condition, $2d\sin\theta=\lambda$, the scattering amplitudes add coherently, and over a narrow band of energy and angle, the x-ray reflectivity from a monochromatic beam can approach 100% (Fig. 5c). The width of the bandpass is determined by the number of diffracting planes, n; dE/E~1/n. Bragg optics are particularly useful for collecting large divergences with small bandpass;

diffraction can occur at Bragg angles roughly 20 times larger than the critical angles for total external reflection mirrors.

Synthetic multilayer mirrors represent an intermediate between Bragg optics and total external reflection mirrors (Fig. 5b). Multilayer mirrors are created by depositing layers with alternating high and low electron density. The reflectivity of these layers can add coherently at the Bragg condition. Typically an x-ray beam penetrates through only ~ 20-200 layers, so the bandpass is much greater than for Bragg reflection optics but much less than for total external reflection optics (Fig. 5b). The Bragg condition for multilayers is typically 5 times greater than the critical angle for total external reflection mirrors and 4 times less than for crystal Bragg angles.

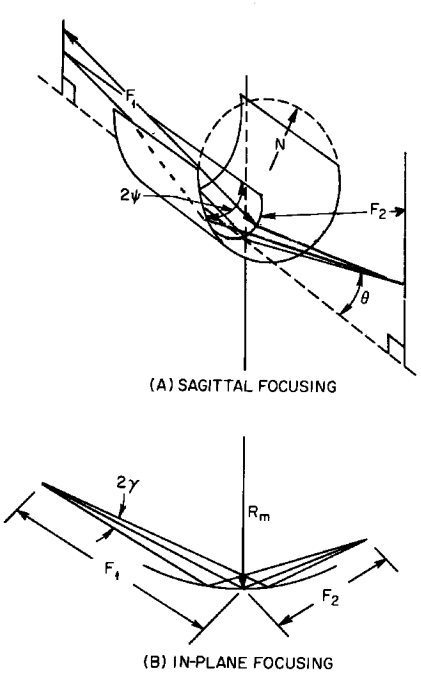

Fig. 6 Sagittal and in-plane focusing.

Basic X-ray Focusing Elements

All current hard x-ray focusing schemes are based on reflective focusing, zone plate condensers , tapered capillaries or some combination of these elements. For both total external reflection and Bragg crystal optics, reflective focusing out of the plane of scatter is called sagittal focusing and focusing in the plane of scatter is referred to as in-plane focusing (Fig. 6).

An x-ray zone plate consists of an amplitude or phase contrast lens constructed from a series of linear or concentric bands. These alter the amplitude or phase of the incident x-ray wave to initiate constructive interference at a focus downstream of the lens (Fig. 7a). A capillary condenser exploits total external reflection within a smooth tapered capillary to condense an x-ray beam(Fig. 7b).

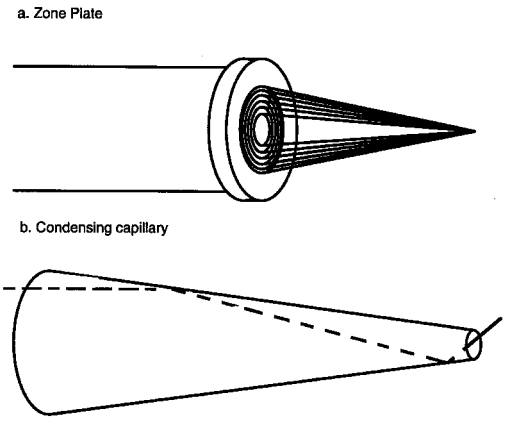

Fig. 7 Zone plate and capillary condensers.

All x-ray microbeam forming optics have a minimum beam divergence which increases as focused spot size decreases. According to the Rayleigh criteria, the diffraction limited minimum divergence through an aperture is,[2]

$$\alpha(mrad) \geq \frac{1.2\lambda(nm)}{D(\mu m)}. \qquad (3)$$

Here α is the angular divergence (mrad), D is the diameter of the aperture (μm) and λ is the x-ray wavelength (nm). For a one micron beam at 5 keV the minimum divergence is about 0.3 mrad. For a one micron beam at 15 keV the minimum divergence is 0.1 mrad. The diffraction limit requires that imaging optics have at least the minimum convergence of Eq. 3 onto the sample to achieve a spot size D. The diffraction limit also means that all apertures add divergence to the beam. The importance of this additional divergence depends on the size of the aperture and the beam divergence onto the aperture.

In addition to the diffraction limit, all imaging optics must satisfy the normal geometrical demagnification criteria to achieve submicron beams.

$$\sigma_{image} \geq \frac{F_2}{F_1}\sigma_{object} = M\sigma_{object} \quad (4)$$

Here σ_{object} is the root-mean-square (rms) source size, σ_{image} is the rms image size, F_2 is object distance and F_1 is the image distance.

Imaging optics must also have small aberrations and beam blurring to achieve a submicron focus. For example the acceptable surface slope errors on reflective optics depends on the RMS object size and the distance to the focusing element. The condition for near geometrical demagnification is that sagittal and in-plane slope errors,$\Delta_{sagittal}$ and $\Delta_{meridional}$, must contribute a beam blur much smaller than the geometrical image.

$$\Delta_{sagittal} \leq \frac{\sigma_{object}}{2F_1 \sin(\theta)}; \qquad \Delta_{meridional} \leq \frac{\sigma_{object}}{2F_1} \quad (5)$$

Although x-ray optics must satisfy the criteria described above to achieve submicron spot size, the *limits* to focusing performance and *efficiency* of various options are best described in terms of phase space concepts.

Phase Space Description of the Source

Both conventional and synchrotron sources are characterized by their x-ray source size, divergence and spectral distributions. It is useful to think of the source properties in terms of independent vertical and horizontal phase spaces defined by co-ordinates of length and angle. For example as shown in Fig. 8, the source vertical-phase space 1/e contour for an undulator at the Advanced Photon Source, APS,is ~170 microns in the space dimension and18 microradians in divergence dimension. This phase space description is only valid over a small energy range but is adequate for this discussion. The area contained within the 1/e contour is referred to as the **vertical source emittance**. In addition to the vertical phase space, the source has a horizontal phase space and a spectral distribution. As mentioned above, these descriptions may not be independent and in general, a source is described by a 5 dimensional phase space which includes the transverse dimensions and divergences, and the x-ray energy distribution.

For a synchrotron source, the source size is determined by the charged-particle beam size, and its projection along the line of sight to the beamline. The source divergence is a convolution of the radiation pattern and the charged particle divergence. [26]

The vertical divergence of the source is highly collimated for all synchrotron sources and the horizontal divergence is also collimated although less so than the vertical divergence. The phase space distributions are often approximated by Gaussian functions in each dimension. The phase space density within a small volume of the five dimensional phase space is refereed to as brilliance.

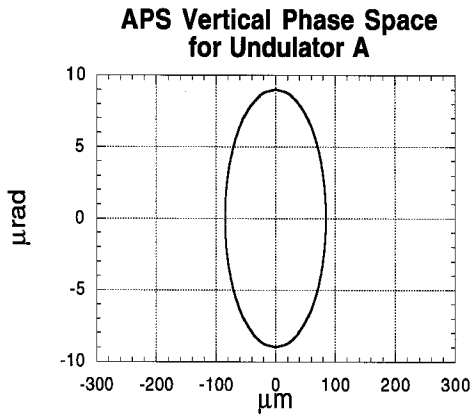

Fig. 8 Vertical Phase Space description for an APS undulator at odd harmonics. The ellipses represent the 1/e contour for the probability distribution.

X-ray source brilliance is a fundamental property of a source and from rather general arguments it can be shown that source brilliance cannot be increased through an x-ray optical system. However the distribution in phase space *can* be controlled by x-ray optics. For example the main advantage of microfocusing optics is to compress the phase space ellipse in the spatial dimension while accepting increased beam divergence. It is efficient to allow the beam divergence to increase up to a maximum set by the particular experiment; this allows the experiment to use a greater fraction of phase space for the same spatial resolution.

Both x-ray microdiffraction and x-ray microfluorescence are ultimately limited by beam brilliance. For both experiments beams with less than 1 μm^2 spatial sensitivity and with crossed divergences on the order of 1-10 $mrad^2$ are desirable.[3] Energy resolution $dE/E \sim 1x10^{-2}$-$1x10^{-4}$ is required depending on the experiment.

The effect of beam transport, apertures and focusing optics on beam brilliance and emittance are illustrated in Fig. 9 for the APS vertical phase space at a odd-order undulator-A harmonic. The source phase space is shown in Fig. 9a as an upright ellipse. As the beam propagates along the beamline it begins to grow vertically due to the initial divergence and reaches a size shown in Fig. 9a at 30 m. The source divergence however does not change and the emittance and brilliance are conserved: the area in the 1/e ellipse and the density are unchanged.

At 30 m from the source we illustrate the effect of an aperture (Fig. 9b). As shown in Fig. 9b, an aperture limits the vertical size of the beam. This constrains both the beam divergence and the source size. To a first approximation beam brilliance is not effected by an aperture, but the emittance is reduced at the cost of flux.

A focusing optical element (Fig. 9c) maps x-ray position into a deflection of the beam to condense the beam. Ideal focusing does not effect emittance or brilliance, but at increasing demagnification, the beam divergence is increased while the effective source size decreases (Fig. 9c). An undulator source can have a vertical beam divergence of ~20 μrad so that demagnifications of 50:1 can achieve small images with less than 1 mrad divergence. Demagnification beyond 50:1 requires reduced emittance (flux cut) to achieve less than 1 mrad divergence.

For real optics, additional beam divergence can be introduced with each optical element. As described previously divergence can be increased by an aperture because of diffraction or by slope errors in a reflecting mirror.

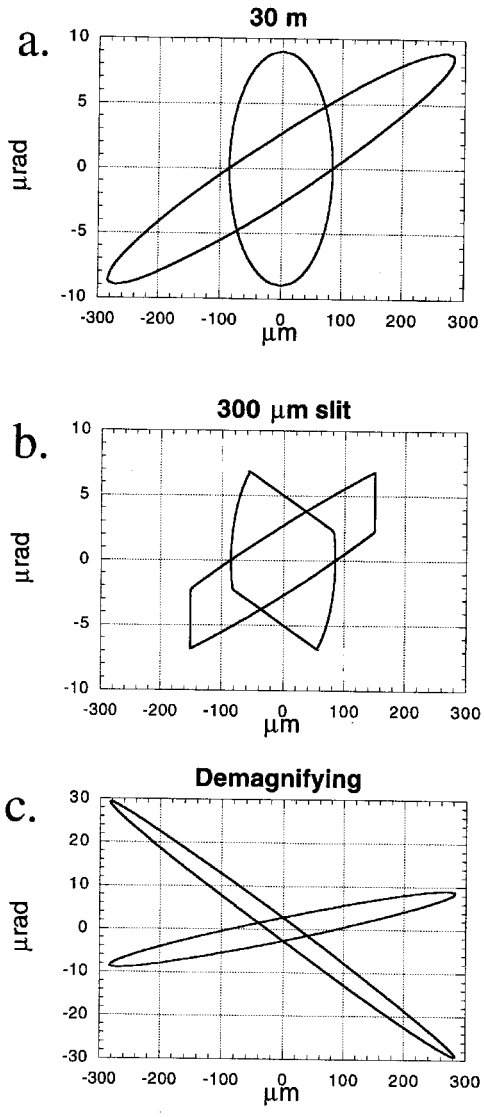

Fig. 9 Phase space description of the vertical phase space for an APS type A undulator comparing the phase space at the source and at 30 m from the source. In a., the phase space ellipse is shown for a simple 30 m propagation in b., with 300 μm slit at 30 m and in c for a demagnifying optic at 30 m.

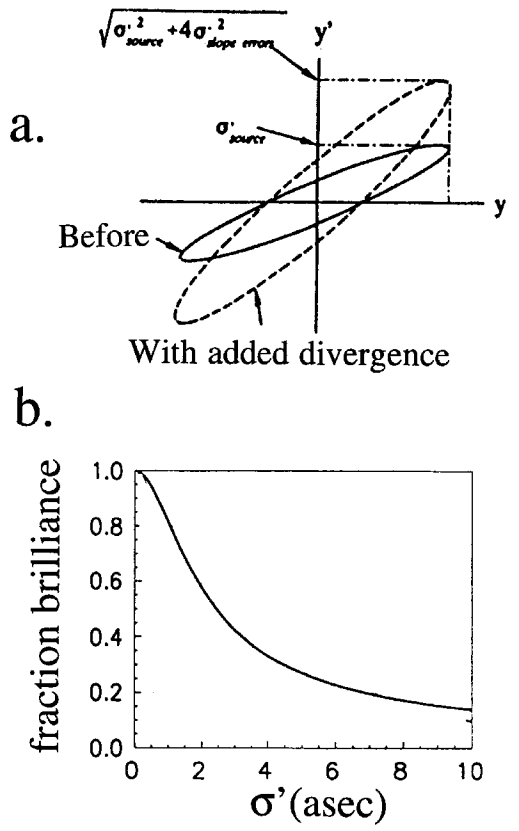

Fig. 10 Divergence added to a the x-ray beam by diffraction or through RMS slope errors increases beam emittance and decreases brilliance. In fig 10a above we add RMS divergence in quadrature to the source RMS divergence. The effect of slope errors on beam brilliance is illustrated in Fig. 10b.

Other possible causes of additional divergence include surface scatter or mosaic crystals planes. Any additional divergence reduces beam brilliance as shown in Fig. 10a for the case of slope errors. With the assumption that the source and contributed divergences have Gaussian distributions, we can model the effect of small slope errors on beam brilliance (Fig. 10b.)

X-ray Microbeam optics

Apertures and pinholes

There are two generic ways to produce an x-ray microprobe beam. One approach is to directly image the source with high demagnification. The alternative is to achieve modest demagnification of the source and then use an aperture to obtain a submicron beam. The aperture can be located either near the sample or at some intermediate focal plane (Fig. 11). If located at an intermediate focal position, then the x-ray beam must be reimaged. Apertures have been successfully used to produce 2-10μm x-ray beams.[6,18] For hard x rays the apertures are typically laser drilled pinholes, adjustable slits, or capillary condensers. Because of the added complexity of reimaging, almost all examples to date have placed the aperture near the sample.

Simple apertures are efficient only if the beam divergence onto the aperture exceeds the diffraction limited divergence. As a consequence, apertures are often used in combination with condensing optics.[20,28] For hard x rays it is difficult to obtain apertures with the needed thickness-to-hole-diameter aspect ratio, and alignment is difficult.[18] Nevertheless, apertures have been widely used to achieve small microprobe beams.[18,20,27,28]

Tapered Capillaries

The use of glass capillaries [14-16] appears to be a promising hybrid between direct imaging and aperturing methods. Research is being conducted in this area at the Cornell High Energy Synchrotron Source (CHESS)[16,29,30] at the Pacific Northwest Laboratory (PNL)[14,31] at Columbia University[32] and at other locations around the world.[33,34]

Tapered glass capillaries currently hold the world record for the smallest x-ray beams. Thiel and Bilderbach[16] have reported a glass capillary with a full-width at half maximum (FWHM) x-ray beam size less than 0.1μm.

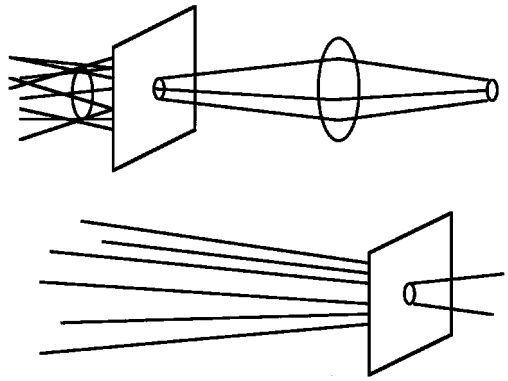

Fig. 11. Two ways to use apertures to increase spatial resolution.

The focusing principle of a tapered glass capillary is illustrated in Fig. 12. X-rays are reflected by total external reflection from a smooth surface if they impinge at angles below the critical angle (Fig. 5). As shown in Fig. 12, a ray at angle α with respect to the capillary axis, makes a first reflection with the inner surface at an angle $\alpha+\beta$ where β is the capillary taper half-angle. The second reflection is at an angle $\alpha+3\beta$ and the nth reflection is at $\alpha+(2n+1)\beta$.

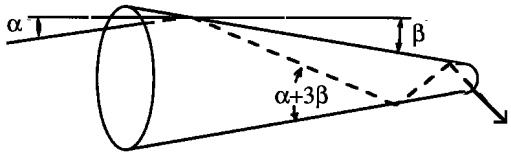

Fig. 12 Schematic of a linearly tapered capillary showing the increase in divergence with multiple reflections. The angle α is the angle of the beam with respect to the capillary axis. The angle β is the half-taper angle of the capillary.

If the angle of incidence exceeds the critical angle for reflection, the x-ray is absorbed at the surface and is not transmitted. Unlike a true lens, capillaries do not image the source: structure in the object is lost with multiple bounces through the capillary and vertical and horizontal phase spaces are mixed.

The maximum throughput efficiency of a condensing capillary can be estimated from the assumption that brilliance is conserved. The maximum divergence in both the vertical and horizontal planes from a capillary is twice the critical angle of reflection for the capillary. As the beam is condensed in a capillary, the divergence must increase until some rays begin to strike the capillary walls at angles beyond the critical angle and are lost. The flux efficiency, P/P_0, for an ideal capillary, therefore, depends on the divergences of the beam at the capillary entrance, σ_h' σ_v' the demagnification,M, and the critical angle, θ_c ,

$$\frac{P}{P_o} \le \frac{\left(M\theta_C\right)^2}{\sigma_v'\sigma_h'} \quad . \qquad (6)$$

This approximation ignores losses during multiple reflections along the capillary. In practice the efficiency of a capillary depends on the taper of the capillary, its mounting, its index of refraction, internal micro-roughness, and its orientation with respect to the incident beam. Few capillaries with near micron beam size even approach the ideal brilliance conserving limit of Eq. 6.

Current state-of-the-art capillaries have beam sizes ranging from 0.1 to 10 microns FWHM and can have theoretical gains in photon flux density of 10^3 or more. Reported flux gains are on the order of 50-1000.[16,29-34]

The length of a glass capillary depends on the taper angle, α, and the diameter, d,at the entrance: $L \sim d/2\alpha$. For even modest sized beams the capillary length becomes quite long. For a linearly tapered capillary the maximum demagnification is simply[14],

$$m_{\max} \ge \left(\frac{\alpha + \beta}{\theta_c} \right). \qquad (7)$$

Here β is the taper angle of the capillary as defined in Fig. 12 and α is the incident angle of the x-ray beam on the inner surface of the capillary. At the APS, the beam divergence relative to the central axis is on the order of $\sigma'_R \approx \sqrt{\sigma'^2_x + \sigma'^2_y}$ = 25μrad. For maximum performance the taper angle, β, should be small compared to σ'_R. We assume a taper angle of 12μrad and $\alpha+\beta \sim 36\mu$rad. The maximum demagnification from equation 7 is therefore on the order of 1:41 at $\theta_c \sim 1.5$ mrad which is the typical critical angle for 20 keV x-rays from a glass capillary.

The useful entrance for a tapered capillary with a 2.5 μ-diam. final opening is therefore of the order of 100 μ-diam and the length of this capillary is 3.3 m. This capillary should achieve a 1600x increase in the flux density and should provide a source with about 1 μ-diam full-width-half-maximum FWHM spatial resolution and 1.5 mrad FWHM-divergence. With a capillary length limit of 1m, a 80 μ-diam. opening yields the highest theoretial flux for a straight taper. Independent of the details of the calculations, is clear that very long and very smooth capillaries are needed to achieve efficient x-ray collection and compression.

Efforts are now underway to optimize the taper shape of glass capillaries. In principle the ideal shape has an elliptical cross section.[31] With an elliptical cross section each ray makes 1 reflection. Capillaries are at a disadvantage compared to total external reflection mirrors because glass has a 2.5 times smaller critical angle of reflection than high Z metals, and because it is not possible to polish the inner surface of the capillary. Capillaries appear to be particularly promising as a final focusing stage of a condensing system. Here small demagnifications (e.g. 10:1) can improve a 10μ-diam. focuss to 1μ-diam.

One disadvantage of small aperture methods such as pinholes and glass capillaries is the need to have the aperture close to the sample. The pinhole or capillary may cover a substantial solid

angle off the sample (if for example the capillary walls are thick). The minimum beam spread is set by diffraction from the aperture (Eq. 3). For example at 20 keV the diffraction limit requires that an aperture be within 14 mm of a sample to preserve a 1 μm beam. More stringent conditions are likely to result in real applications. The diffraction limited distance between an aperture and the sample decreases as the square of the aperture diameter. Therefore a 0.1 μm-diam. aperture or capillary must be within 140 μm of the sample to preserve spot size.

A glass capillary with a critical angle of 1.5 mrad will have an rms exit beam of ~0.8 mrad. To preserve a submicron beam, the end of the capillary must be less than 1.2 mm from the sample. Glass capillaries appear to be better suited than pinholes as a final demagnifying stage: they have inherently high aspect ratio of thickness to diameter.

Ellipsoidal Total Reflecting Mirrors

The alternative to aperturing the beam is to directly image the beam to a submicron spot. With a FWHM source size of ~0.2 x 0.6 mm^2 at the Advanced Photon Source (APS) the demagnification required to produce a 1 μm spot is 200:1 in the vertical and 600:1 in the horizontal. At the Advanced Light Source (ALS) demagnifications of 60:1 and 200:1 will achieve 1 μm resolution. For specular reflection from a single mirror, ellipsoidal surfaces of revolution produce the smallest aberrations of the image. An ellipsoid combines sagittal (out-of-plane) and meridian (in-plane) focusing in one doubly curved optical element (Fig. 6). At the European Synchrotron Radiation Facility (ESRF) an ellipsoidal mirror on their microprobe beamline is used to develop a 100 μm^2 focal spot.[28]

A current limit to demagnification with ellipsoidal mirrors arises from the difficult fabrication of highly asymmetric optics with acceptable surface roughness and figure errors. A discussion of this limit must consider the surface and figure accuracy requirements of x-ray mirrors.

The mirror finish required to preserve brilliance, can be divided into at least two distinct regimes. At short spatial frequencies, surface roughness controls the scatter of the beam. At long spatial frequencies, slope errors (figure error) cause the image to be blurred. An excellent summary of x-ray mirror requirements is given by Freund.[35]

The tolerance required for a mirror depends primarily on the source size, the distance from the mirror to the source, and the x-ray wavelength. Consider, for example, the figure precision required for an APS mirror.

The APS vertical source size, σ_y is about 85 μm and the distance from the source to a first mirror, F_1, is on the order of 30 m. If the slope deviates from the ideal figure with an root-mean-square rms deviation, σ'_s, the image will be blurred by $2\sigma'_s MF_1$. The slope error must, therefore, have a standard deviation of less than $\sigma_y/2F_1$. At the APS this represents a standard deviation of 1.4 μrad. Slope errors are most important for mirror length scales greater than ~3mm.

The grating equation, $\lambda=\theta_s\theta_i d$, can be used to estimate the dimension, d, below which surface roughness scatters outside the image region. With an incident beam angle, θ_i, of 3 mrad and a scatter angle, θ_s, due to roughness less than 2.8 μrad, dimensions d(mm)<12λ(Å) will scatter outside the geometrical image. Therefore at 10 keV, spatial frequencies below 1 cm can scatter out of the geometrical image.

The total intensity into the geometrically demagnified beam can be estimated by,

$$I = I_O \exp\left(\frac{-4\pi\sigma_s\theta}{\lambda}\right)^2 . \qquad (8)$$

Here σ_s is the RMS surface roughness below spatial frequencies of 1 cm. For 90% power in the geometrical image and with θ~3 mrad, the surface roughness below 1 cm must satisfy $\sigma_s(\text{Å}) \sim 8.6\lambda(\text{Å})$.

To illustrate the technical challenge of a microfocusing ellipsoidal mirror we calculate the asymmetric radii of an ellipsoidal condensing mirror. The sagittal, R_s, (Fig. 6a) and meridional. R_m, (Fig. 6b) radii of a ellipsoidal mirror are given by,

$$R_s = 2F_1F_2 \sin\theta/(F_1 + F_2), \quad (9a)$$

$$R_m = R_s/\sin^2\theta \ . \quad (9b)$$

Here, F_1 is the object (source) distance, F_2 is the image (sample) distance and θ is the scattering angle. For F_1 of 70 m, and $\sin\theta \sim 0.008$ (specular mirror), and $R_s \sim 1$ cm, we find a maximum demagnification of 110:1. Even if such a highly asymmetric mirror could be manufactured, the magnification will yield a focal spot size of 6 x 1.8 μm at the APS. To achieve 600:1 demagnification, the sagittal radius would be ~ 1.8 mm. Both the surface roughness and figure tolerance of such a mirror exceeds existing manufactoring capabilities for such an asymmetric mirror. Ellipsoidal mirrors are probably a poor choice for direct microfocusing, although they might be combined with apertures or capillaries as at the ESRF.[28]

Kirkpatrick-Baez Total Reflection Mirrors

A possible microfocusing option which uses total external reflection mirrors combines crossed meridional mirrors in the Kirkpatrick-Baez, KB, geometry.[36] This geometry is illustrated in Fig. 13. Like the ellipsoidal mirror described above, a total-external-reflection KB mirror system has the advantage of being broad bandpass. The bandpass and bandwidth can, therefore, be controlled by an upstream monochromator of traditional design.

Until recently, most KB mirror systems used cylindrical or spherical mirrors.[36,37] These mirrors were adequate for focusing to about 10 μm-diam. spots, but were limited by spherical aberration. Beams as small as ~2 μm were demonstrated, but with very small acceptance.

Although elliptical mirrors have long been recognized as being more ideal, it is difficult to manufactor even a simple elliptical mirrior with x-ray quality surface roughness; elliptical mirrors cannot be polished with sub nanometer rms roughness. Recently there have been a number of methods proposed and demonstrated for obtaining elliptical mirrors with x-ray quality figure and surface roughness.[39-40] These include bending schemes for refiguring flat mirrors and methods for modifying an x-ray quality cylinder. It is now possible to say that KB mirror systems can routinely focus to near micron beams and should achieve submicron resolution with further refinement. Ray tracing results indicate that intense x-ray beams with cross sections of less than 0.04 μm^2 are achievable.

Kirkpatrick-Baez optics make sense for many applications because they can efficiently use the available phase space. Assuming negligible figure error and surface roughness, the main limitation to KB optics is the critical mirror angle which limits beam convergence (divergence). With total external reflection optics the maximum convergence angles achievable is about 1/2 to 2/3 of the mirror angle. This divergence limit sets a lower limit on the minimum spot size which can be achieved with KB optics (Eq. 3). Below 22 keV, a rhodium coated total-external-reflecting KB system cannot focus to less than ~0.025 μm-diam. The restricted angular acceptance of KB total external reflection mirrors is also somewhat limiting for fluorescence analysis of high Z materials where

convergence angles of 5-10mrad are desirable. Nevertheless these mirrors are highly promising for both x-ray microdiffraction and x-ray microfluorescence.

Kirkpatrick-Baez Multilayer Mirrors

One practical approach for extending KB microfocusing to smaller probe sizes and with larger convergence angles, is to use two crossed multilayer mirrors in the KB geometry. Several of these multilayer systems have been built and tested on synchrotron radiation facilities.[7,36-38] These devices have been pioneered by Jim Underwood, Al Thompson and their colleagues at Lawrence Berkeley Laboratory. The mirrors must again be elliptical to achieve submicron probe size and should have graded d spacings to match the bandpass of both mirrors.[1,3] Multilayer focusing combines some monochromatization, determined by the number of reflecting layers, with focusing so that for some applications an upstream monochromator is not needed.

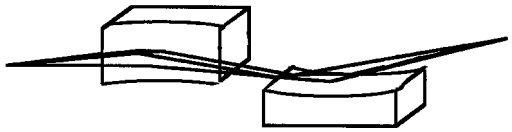

Fig. 13 Kirkpatrick-Baez focusing mirror pair.

In comparison to a specular reflecting system, a multilayer system has approximately five times larger reflecting angles. This means that these devices can collect larger divergences especially at high energies (larger aperture). A disadvantage of multilayer focusing is the difficulty of tuning energy beyond the bandpass of the multilayer and a need to grade the d spacing to compensate for different scattering angles along the multilayers. Another disadvantage of KB multilayer mirrors is their low reflectivity compared with total-external reflection mirrors. Multilayer reflectivity ranges from about 30-60% whereas total external reflection mirrors have about 70-90% reflectivity.

Zone Plates

Another promising technology is the use of zone plates for hard x-ray imaging. Zone plates can use either phase or amplitude modification to condense an x-ray beam. With amplitude (opaque) zones, a theoretical efficiency of only 10% is possible. With phase modification an efficiency of up to 40% can be achieved. Almost all hard x-ray zone plates use a combination of phase and amplitude modification.

Zone plates have been used to focus soft x rays with great success.[41] Their application to hard x rays has been limited by the difficulty of obtaining the required high-aspect ratio. This problem is similar to the difficulty of procuring high aspect apertures for x rays. The construction of high-aspect-ratio zone plates was first achieved by Richard Bionta and associates at Lawrence Livermore National Laboratory using a sputtered-slice technique.[42] With this technique, a high Z wire has concentric layers of alternating Z deposited. The resulting "jelly roll" structure is sliced to create the x-ray lens (Fig. 14). A state-of-the-art phase zone plate can be constructed by this method with a ~0.3-mm aperture and a 30-cm focal length and with ~30% efficiency over a small energy range. The ultimate resolution of a zone plate depends on the thickness of the last zone and on the depth of the zone plate.[43] It is possible that zone plates with resolutions down to 0.1 μm or less can be fabricated. The aperture of the zone plate can be reduced to decrease the focal length. With current jelly roll techniques it should be possible to fabricate a zone plate with a 10 cm focal length and with a 100 μm-diam. aperture. At 60 m from the source, such a zone plate would have a 600:1 demagnification.

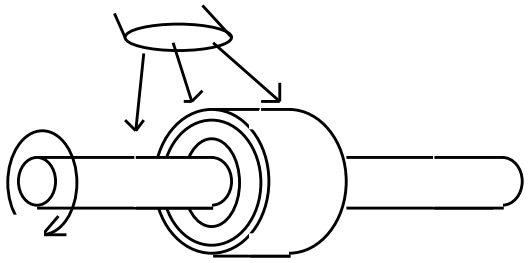

Fig. 14 Jelly roll or sputter/slice technique for the fabrication of hard x-ray zone plates.

Compared to the other optics discussed, zone plates are much easier to align although their focused intensity distribution is complicated and requires secondary apertures to obtain a clean beam. Even greater demagnifications (at reduced efficiency) are possible with the zone plates used in higher orders.

Recent advances in lithographic techniques have also been used to develop x-ray zone plates. Yun[43] has described a lithographic zone plate with 0.25 μm outer line width and a 60-μm-diam. This zone plate is capable of achieving very small spot size.[10] A zone plate with 0.2 μm spatial resolution is planned for early operation on the APS.[44]

Performance of zone plates fabricated by a lithographic method and a sputtering/slicing method have been characterized using synchrotron radiation.[10] These zone plates have been used successfully to focus synchrotron x rays to a small focal spot with focusing efficiency close to that predicted theoretically. For a Ni zone plate fabricated with the lithographic technique, a focusing efficiency of 33% was experimentally measured and a diffraction-limited focal spot was obtained. Both lithographic and sputter/slice techniques can in principle yield microbeams with ~0.1 μm resolution.

Two practical limits with zone plates help to put their performance in perspective with the previous optics. The maximum acceptance of a zone plate is limited by the ability to produce fine zones at the edge of the zone plate. The radius R_K for the Kth zone is approximately given by,[45]

$$R_K^2 \approx \sqrt{Kf\lambda}. \qquad (9)$$

Here f is zone plate focal length and λ is the x-ray wavelength. We assume that zones with 0.2 μ spacing can be fabricated and that a focal length of 0.135 m is required to achieve a 1.0 μm^2 probe area (2.7 x 0.37 μm^2). From Eq. 9 we can therefore estimate the maximum useful zone aperture to be about 120 μm-diam. Zone plates with efficiencies up to 30% are possible with current technology. As the probe dimension decreases, the aperture size rapidly decreases. For example, when both the vertical and horizontal probe size must be less than 1 μm, the maximum useful aperture for an APS zone plate is only 15μm-diam.

Another limitation of zone plates is their inherent chromatic aberration. The focal length of a zone plate is inversely proportional to the wavelength. Therefore, as x-ray energy increases, the zone plate focal length also increases. This chromatic aberration limits the useful aperture of a zone plate for a given bandpass and a given focal spot size. For small bandpass ΔE/E and an aperture diameter A, the chromatic blur of a zone plate is given by,

$$\sigma_{chromatic} \sim \frac{A}{2}\,\frac{\Delta E}{E} \quad . \qquad (10)$$

Hence, with a 1% bandpass the aperture of a zone plate must be less than 100 μm to achieve a 1-μm-diam. focal spot. This limits the phase space acceptance of a zone plate with 1% ΔE/E below that for mirrors considered previously. For scanning purposes, with small bandpass, it may be possible to maintain the zone plate image position by a precision linear translation of the zone plate. However,

very small transverse motions of the plate can be tolerated during translation. For small fixed bandwidths, however, the zone plate technology may be the first to routinely achieve resolutions of 0.1 μm.

Bragg-Fresnel Optics

Bragg Fresnel optics are a hybrid which combines single crystal reflection and zone plate optics. These devices are currently being pursued by scientists at the European Synchrotron Radiation Facility and have already achieved submicron focused beam sizes.[12,13,46,47] With Bragg-Fresnel optics a phase contrast Fresnel pattern is layed down on a single Bragg crystal or multilayer by etching steps in the crystal surface (Fig. 15). Phase contrast is provided by the difference in path length to the top and bottom of the steps. This design has the advantage of being intrinsically a phase contrast design, and the contrast relationship remains fixed with energy. In addition the construction of the zones is simplified because they are supported on a massive single crystal. The narrow (Bragg) energy bandpass intrinsic to Bragg-Fresnel optics, ensures that chromatic aberration is negligible. Reported Bragg-Fresnel performance has achieved submicron dimensions (0.8 μm) for a linear condenser[45] and 5 x 2.5 μm^2 for a point focusing Bragg-Fresnel lens.[46]

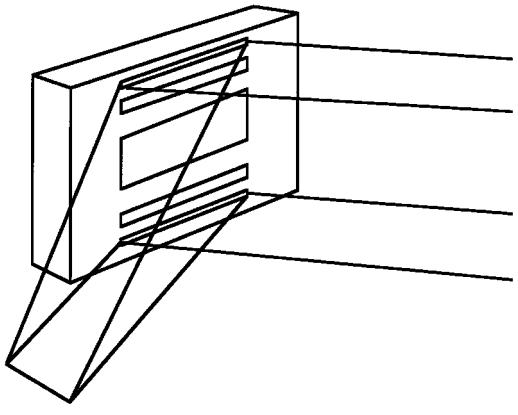

Fig. 15 Bragg Fresnel focusing elements.

Bragg-Fresnel focusing options are quite general and can include single focusing or double focusing. and can be combined into KB like focusing systems.

Summary

A qualitative summary of the relative merits and challenges for various microbeam forming methods are given in Table 1. There are at least four methods capable of efficiently achieving submicron beams. These include tapered capillaries, KB mirror optics, zone plates and Bragg-Fresnel optics. Tapered capillaries can achieve the smallest beam dimensions but are less efficient than KB mirror systems. In general capillary optics will suffer from efficiency losses as capillary figure and surface roughness deviate from ideal, but will achieve near ideal spatial resolution.

KB total-external-reflection mirror optics are highly desirable for applications requiring tunability and high efficiency. These systems are more likely than capillaries to fall below ideal performance in spatial resolution but are more likely than capillary systems to have near ideal flux performance. One advantage with KB mirrors is the ability to achieve symmetric spatial resolution by using different magnifications for the vertical and horizontal focusing mirrors.

KB multilayer mirrors can achieve the highest flux of any system and are especially well suited to fluorescence experiments where bandpasses on the order of a few percent can be desirable. KB mirrors however are not well suited for tuning beyond the natural bandpass of the mirrors.

Zone plates and Bragg-Fresnel optics are especially promising for fixed wavelength applications. The achievable performance of both focusing devices is very similar although Bragg-Fresnel lenses are at a small advantage because they are intrinsically phase constrast devices. Zone plates can be moved to provide a fixed focus as wavelength is tuned but such

motions must be very precise to preserve the image location.

In addition to the focusing systems shown in Table 1, there are various combinations of optical elements which can achieve submicron probe dimensions. The systems shown in Table 1 however, show the most promise for the future.

Table 1. Relative merits of X-ray Microbeam Forming Options at 20 keV with an APS type A undulator operating with 100 mA ring current.

Optics	Achievable Spatial Resolution	Divergence (mrad)	Flux with 1-μm^2 spot 0.15% bandwidth	Bandpass	Scannable
Capillary	0.1-5μm	~1.5	1.6×10^{10}	high E filtered to 20 keV	Yes
KB Mirror	0.5-5 μm	~ 0.5	5.4×10^{10}	White to 22 keV	Yes
KB Multilayer	0.5-5 μm	~ 2	1.9×10^{11}	1-5%	Difficult
Zone Plate	0.2-5 μm	~0.5	5.7×10^{10}	1×10^{-4}	Possible
Bragg-Fresnel	0.2-5 μm	~ 0.5	5.7×10^{10}	1×10^{-4}	Difficult

Acknowledgment

This research is sponsored by the Division of Materials Sciences, U.S. Department of Energy under contract DE-AC05-96OR22464 with Lockheed Martin Energy Research Corporation.

References:

1. D.H. Bilderback, B.M. Lairson, T.W. Barbee, Jr., G.E. Ice and C.J. Sparks, *Nucl. Instr. and Meth.* **208**, 251 (1983).

2. M.R. Howells and J.B. Hastings, *Nucl. Inst. and Meth.* **208**, 379 (1983).

3. G.E. Ice and C.J. Sparks, *Nucl. Instr. and Meth.* **222**, 121 (1984).

4. C.J. Sparks and G.E. Ice, *Mat. Res. Soc. Symp. Proc.* **143**, 223 (1989).

5. A.C. Thompson, K.L. Chapman, G.E. Ice, C.J. Sparks, W. Yun, B. Lai, D. Legnini, P.J. Vicarro, M.L. Rivers, D.H. Bilderback and D.J. Thiel, *Nucl. Instr. and Meth.* **A319**, 320 (1992).

6. K.W. Jones nd B.M. Gordon, Anal. Chem. **61**, 341 (1989).

7. J. H. Underwood, A.C. Thompson, J.B. Kortright, K.C. Chapman and D. Lunt, submitted *Rev. Sci. Inst.* (1996).

8. B.X. Yang submitted *Rev. Sci. Inst*. (1996).

9. M.R. Howells and D. Lunt, *Opt. Eng*. **32**, 1981 (1993).

10. W.B. Yun, B. Lai, D. Legnini, Y.H. Xiao, J. Chrzas, K.M. Skulina, R. M. Bionta, V. White and F. Cerrina, *SPIE* **1740**, 117 (1992).

11. R.M. Bionta, E. Ables, O. Clamp, O.D. Edwards, P.C. Gabriele, K. Miller, L.L. Ott, K.M. Skulina, R. Tilley, T. Viada, *Opt. Eng.* **29**, 576 (1990).

12. A.A. Snigirev. I.I. Snigireava, C. Riekel, A. Miller, L. Wess, T. Wess, *Journal de Physique* IV, **3** Suppl.JPIII, N12, 403 (1993).

13. J. Chavanne, P. Elleaume, E. Tarazona, Y.M. Hartman, I.I. Snigireva, A.A. Snigirev, *Rev. Sci. Inst*. **65**, 1959 (1994).

14. E. A. Stern, Z. Kalman, A. Lewis and K. Lieberman, *Appl. Opt*. **27**, 5135 (1988).

15. S. Larsson and P. Engström, *Adv. in X-ray Analysis*, **35** 1019 (1992).

16. D. H. Bilderbach, S. A. Hoffman, and D. J. Thiel, *Science* **263** 201 (1994).

17. C. J. Sparks, "X-ray Fluorescence Microprobe for Chemical Analysis", in *Synchrotron Radiation Research*, edited by H. Winick and S. Doniach, (Plenum Press 1980) 459.

18. R. Rebonato, G.E. Ice, A. Habenschuss, J.C. Bilello, *Phil. Mag A*, **60**, 571-583 (1989).

19. N. Yamamoto and S. Sakata Jpn J. *Appl. Physics* **34**, 664 (1995).

20. P. Horowitz and J. A. Howell, *Science* **178**, 608 (1972).

21. C.J. Sparks, Jr. and J.B. Hastings, *Oak Ridge National Laboratory Report* ORNL-5089 (1975).

22. C.J. Sparks, Jr. S. Raman,H.L. Yakel, R.V. Gentry and M. O. Krause, *Phys. Rev. Lett.* **38**, 208 (1977).

23. C.J. Sparks Jr., S. Raman, H.L. Yakel, R.V. Gentry and M.O. Krause, *Phys. Rev. Lett.* **40**, 507 (1978).

24. R.V. Gentry, T.A. Cahill, N.R. Fletcher, H.C. Kaufmann, L.R. Medsker, J.W. Nelson and R.G. Flocchini, *Phys. Rev. Lett.* **37**, 11 (1976).

25. A. Franks, *Sci. Prog. Oxf.* **64**, 371-422 (1977).

26. E.D. Johnson, S.L. Hulbert and L.E. Berman, *BNL-47058* Informal Report.

27.M. Rivers, S.R. Sutton, and B.M.Gordon, *Mat. Res. Symp. Proc.* **143**, 285 (1989).

28. C. Riekel , *J. de Physique IV*, **C8**, 403 (1993); C. Riekel, P. Bosecke and M. Sanchez del Rio, *Rev. Sci. Instr.*. **63**, 974 (1992).

29. S.A. Hoffman, D.J. Thiel, and D.H. Bilderback, *Optical Engineering* **33**, 303 1994

30. D.J. Thiel, E.A. Stern, D.H. Bilderback, A. Lewis, *Physica B* , **158**, 314 (1989).

31. D.L. Brewe, S.M. Heald, B. Barg, F.C.Brown, K.H. Kim and E.A. Stern, to be published *SPIE proceedings* (1995).

32. G.S. Cargill III, K. Hwang, J.W. Lam, P.C. Wang, E. Liniger and I.C. Noyan, *SPIE* **2516** (1995).

33. N. Yamamoto and Y. Hosokawa, Jpn. J. Appl. Phys. **27**, L2203 (1988).

34. P. Engstrom, S. Larsson, A. Rindby, A. Buttkewitz, S. Garbe, G. Gaul, A. Knochel and F. Lechtenberg, *Nucl. Inst. and Meth.* **A302**, 547 (1991).

35. A. Freund*Rev. Sci. Instr.* **60** 1549 (1995).

36. P. Kirkpatrick and V. Baez, *J. Opt. Soc. Am* . **38**, 766 (1948).

37. Y. Suzuki, F. Uchida, and Y. Hirai, *Photon Factory 1989 Annual Report Proposal 89-Y015*.

38. A. Thompson, *Center for X-ray Optics 1989 Annual Report*, **LBL-28001**, (1990).

39. M. Howells, *Opt. Eng.* **34**, 410 (1995).

40. M. Howells, LBL Report **LBL-34750** (1993).

41. D. Sayre, M. Howells, J. Kirz, and H. Rarbeck (eds.), *X-Ray Microscopy II*, Springer Verlag, New York (1987).

42.R. M. Bionta, E. Ables, K. J. Cook, O. D. Edwards, P. C. Gabriele, A. F. Jankowski, D. M. Makawiecki, L. L. Ott, and N. Thomas, SPIE **984**, 247 (1988).

43. B. Lai, W.B. Yun, D. Legini, Y. Xiao, J Chrzas, P.J. Viccaro, V. White, S. Bajikar, D.Denton, F.Cerrina, E. Difabrizio, M. Gentili, L. Grella, M. Baciocchi, *Appl. Phys. Lett.* **61,** 1877 (1992).

44. W. B. Yun, private communication.

45. W. B. Yun, P.J. Vicarro, B. Lai and J Chrzas, *Rev. Sci. Inst.* **63**, 582 (1992).

46. S.M. Kuznetsov, I.I. Snigireva, A.A. Snigirev, P. Engström and C.Riekel, *Appl. Phys. Lett.* **65**, 827 (1994).

47. T. Tarazona, P Elleaume, J. Chavanne, Y. M. Hartman, A.A. Snigirev and I. I. Snigireva, *Rev. Sci. Instr.* **65**, 1959 (1994).